http://dx.doi.org/10.5012/bkcs.2012.33.1.48

Synthesis, Structure, and Reactivity of the $[Fe_4S_4(SR)_4]^{2-}$ (R = 2-, 3-, and 4-Pyridinemethane) Clusters

Yujin Kim and Jaehong Han*

Metalloenzyme Research Group and School of Biosciences, Chung-Ang University, Anseong 456-756, Korea
**E-mail: jaehongh@cau.ac.kr*
Received October 6, 2011, Accepted October 26, 2011

The $[Fe_4S_4]^{2+}$ clusters with 2-, 3-, and 4-pyridinemethanethiolate (S2-Pic, S3-Pic, and S4-Pic, respectively) terminal ligands have been synthesized from the ligand substitution reaction of the $(^nBu_4N)_2[Fe_4S_4Cl_4]$ (**I**) cluster. The new $(^nBu_4N)_2[Fe_4S_4(SR)_4]$ (R = 2-Pic; **II**, 3-Pic; **III**, 4-Pic; **IV**) clusters were characterized by FT-IR and UV-Vis spectroscopy. Cluster **II** was crystallized in the monoclinic space group $C2/c$ with a = 24.530 (5) Å, b = 24.636(4) Å, c = 21.762(4) Å, β = 103.253(3)°, and Z = 8. The X-ray structure of **II** showed two unique 2:2 site-differentiated $[Fe_4S_4]^{2+}$ clusters due to the bidentate-mode coordination by 2-pyridinemethanethiolate ligands. Cluster **III** was crystallized in the same monoclinic space group $C2/c$ with a = 26.0740(18) Å, b = 23.3195(16) Å, c = 22.3720(15) Å, β = 100.467(2)°, and Z = 8. The 3-pyridinemethanethiolate ligand of **III** was coordinated to the $[Fe_4S_4]^{2+}$ core as a terminal mode. Cluster **IV** with 4-pyridinemethanethiolate ligands was found to have a similar structure to the cluster **III**. Fully reversible $[Fe_4S_4]^{2+}/[Fe_4S_4]^{+}$ redox waves were observed from all three clusters by cyclic voltammetry measurement. The electrochemical potentials for the $[Fe_4S_4]^{2+}/[Fe_4S_4]^{+}$ transition decreased in the order of **II**, **III** and **IV**, and the reduction potential changes by the ligands were explained based on the structural differences among the complexes. The complex **III** was reacted with sulfonium salt of $[PhMeSCH_2$-p-$C_6H_4CN](BF_4)$ in MeCN to test possible radical-involving reaction as a functional model of the $[Fe_4S_4]$-SAM (*S*-adenosylmethionine) cofactor. However, the isolated reaction products of 3-pyridinemethanethiolate-*p*-cyanobenzylsulfide and thioanisole suggested that the reaction followed an ionic mechanism and the products formed from the terminal ligand attack to the sulfonium.

Key Words : Electrochemistry, Fe/S cluster, Site-differentiated, Synthesis, X-ray structure

Introduction

While the early model studies of the catalytic Fe/S cluster enzymes were focused on the synthesis of the FeMo cofactor of nitrogenase,[1-3] recent synthetic efforts aim to synthesize various biological Fe/S clusters found in metalloenzymes, such as biotin synthase, aconitase, sulfite reductase, and acetyl-CoA synthase. In these enzymes, different core structures and metal compositions, as well as with various coordination environments of the Fe/S clusters, are observed. For examples, incomplete cuboidal Fe_3S_4 cluster found from aconitase-type proteins was synthesized by anchoring Fe/S clusters in the large tridentate ligands[4] and for the synthesis of the heterometal-incorporated Ni/Fe/S clusters found in [NiFe]-hydrogenase, mononuclear Ni complexes were reacted with the ready-made Fe/S clusters.[5] Similar approach was also adopted for the synthesis of C-cluster of acetyl-CoA synthase.[6]

Even for the typical Fe_4S_4 enzymes, one or more Fe centers of the catalytic Fe_4S_4 cluster are usually coordinated to the nonconventional amino acid residues (other than cysteine or histidine), or to the other organic/inorganic cofactors. For instances, IspH in the non-mevalonate pathway, catalyzing the formation of isopentenyl diphosphate,[7] and the radical SAM (*S*-adenosylmethionine) enzymes[8] are characterized to have 1:3 site-differentiated Fe_4S_4 cluster with the unique Fe site coordinated to the substrate and SAM, respectively. In the case of NirA sulfite reductase, the Fe_4S_4 cluster is coordinated to siroheme through the bridging cysteinyl ligand at the unique Fe site of the Fe/S cluster.[9] Accordingly, functionalization of the terminal ligands of the synthetic Fe/S clusters is necessary for the bioinorganic study of these site-differentiated Fe/S clusters.

In this paper, we report the synthesis, structures and physical properties of $[Fe_4S_4]^{2+}$ clusters with pyridinemethanethiolate ligands, as well as the reactivity study of sulfonium cleavage which may be relevant to the radical SAM enzyme.[10] The justification for pyridinemethanethiolate derivatizations of the Fe_4S_4 cluster is to provide Lewis acid binding sites at the terminal ligands with the pyridyl group. Although multidentate pyridyl ligands have been used for the synthesis of many transition metal complexes,[11-14] synthesis of the Fe_4S_4 clusters with pyridinemethanethiolate ligands has never been reported to the best of our knowledge.

Experimental Section

General. All experiments and reactions were carried out under a dinitrogen atmosphere using standard Schlenk line techniques or in an inert atmosphere glove box. All solvents were distilled under dinitrogen and nitrogen gas was bubbled through before use. Acetonitrile was pre-dried over

oven-dried molecular sieves and distilled over CaH_2. Ethyl ether and THF were pre-dried over Na ribbon and further purified by the sodium-benzoketyl method. Water was degassed under vacuum with stirring. 2-, 3-, and 4-picolyl chloride hydrochloride were purchased from TCI (Tokyo, Japan), and elemental sulfur, (^{n}Bu$_4$N)Cl·xH_2O and anhydrous $FeCl_2$ were purchased from Sigma-Aldrich (Sigma Aldrich Co, USA). Thiourea, NaOH and Na metal were purchased from Samchun Chemical (Samchun pure chemical co, Korea). All chemicals used for synthesis were used without further purification. The (^{n}Bu$_4$N)$_2$[$Fe_4S_4Cl_4$] cluster (**I**) was prepared according to the published method.[15]

FT-IR spectra were collected on a Shimadzu FT-IR 8400S FT-IR spectrometer in KBr pellets and the spectra were corrected for KBr background. For far-infrared spectra measurements, Nicolet Magna 750 FT-IR spectrometer at CRF in Chung-Ang University was used. Elemental analysis were performed in the Organic Reaction Center at Sogang University and the data were corrected using acetanilide as a standard. Electronic spectra were recorded on a Scinco-3100 UV-Visible spectrophotometer. NMR spectra were obtained on a 300 MHz Varian Gemini 2000 NMR spectrometer. EI-Mass spectra were collected on an Autospec Mass Spectrometer by direct injection. Cyclic voltammetry (CV) was performed on a Princeton Applied Research Versa STAT 3 potentiostat with a K0264 microcell kit at GRRC in Chung-Ang University. Three electrodes consisted of a Pt working electrode, a Pt auxiliary electrode and a Ag/AgCl as a reference electrode. Measurements were carried out with 0.05 M of complexes in acetonitrile using 0.1 M of (^{n}Bu$_4$N)(PF_6) as supporting electrolyte. The $E_{1/2}$ of ferrocene oxidation was observed at +0.455 V under the conditions.

2-, 3-, and 4-Pyridinemethanethiol (HS2-Pic, HS3-Pic, and HS4-Pic) were synthesized according to the published method with slight modifications.[16] To a solution of 2-picolyl chloride hydrochloride (2.34 g, 14.24 mmoL) in 40 mL of degassed H_2O was added thiourea (1.17 g, 15.32 mmoL), and the reaction mixture was stirred for 30 min at 85-89 °C under N_2 atmosphere. The reaction mixture was then cooled to 5 °C, and NaOH (1.71 g, 42.64 mmoL) was added. After NaOH addition, the resulting mixture was stirred for 6 hrs under N_2 atmosphere at room temperature. The reaction mixture was washed with three portions of 150 mL of *tert*-butylmethyl ether and cooled to 5 °C. By adding 1 M HCl solution dropwise, the solution was neutralized to pH 7. The product was extracted with three portions of 150 mL of CH_2Cl_2. The combined CH_2Cl_2 solution was washed with 150 mL of brine, dried with anhydrous $MgSO_4$, and evaporated to provide 0.724 g (5.78 mmoL, 41% yield) of oily 2-pyridinemethanethiol. R_f = 0.63 (acetone:hexanes = 2:1). ^{1}H-NMR (300 MHz, $CDCl_3$, ppm) 3.84 (*d*, *J* = 3.3 Hz, 2H, CH_2), 7.21 (m, 2H, Pyr), 7.64 (m, 1H, Pyr), 8.53 (m, 1H, Pyr). 3-Pyridinemethanethiol. R_f = 0.68 (acetone:hexanes = 2:1). ^{1}H-NMR (300 MHz, $CDCl_3$, ppm) 1.86 (*t*, *J* = 7.7 Hz, 1H, SH), 3.73 (*d*, *J* = 7.7 Hz, 2H, CH_2), 7.26 (m, 1H, Pyr), 7.68 (m, 1H, Pyr), 8.49 (m, 1H, Pyr), 8.55 (m, 1H, Pyr). 4-Pyridinemethanethiol. R_f = 0.56 (acetone:hexanes = 2:1). ^{1}H-NMR (300 MHz, $CDCl_3$, ppm) 1.81 (*t*, *J* = 7.7 Hz, 1H, SH), 3.70 (*d*, *J* = 7.7 Hz, 2H, CH_2), 7.27 (*d*, *J* = 5.5 Hz, 2H, Pyr), 8.55 (*d*, *J* = 5.5 Hz, 2H, Pyr).

Sodium 2-, 3-, and 4-Pyridinemethanethiolate (NaS2-Pic, NaS3-Pic, and NaS4-Pic). To the solution of Na (0.1595 g, 6.94 mmoL, 1.2 eq) in anhydrous MeOH (10 mL) was added 2-pyridinemethanethiol (0.724 g, 5.78 mmoL) under inert atmosphere. The solution was stirred for 1 hr, and the solvent was removed *in vacuo*. The product was washed with ether and dried to result in white powder of sodium 2-pyridinemethanethiolate (0.79 g, 5.37 mmoL, 93% yield). FT-IR (KBr, cm^{-1}) 3072(s), 2999(s), 2918(s), 2898(s), 2825(m), 1632(vs), 1589(vs), 1566(vs), 1471(vs), 1427(vs), 1373(m), 1300(m), 1255(m), 1194(s), 1149(m), 1101(w), 1085(m), 773(m), 740(vs), 711(s), 628(m), 600(m), 582(m). Sodium 3-pyridinemethanethiolate. (0.81 g, 5.50 mmoL, 95% yield) FT-IR (KBr, cm^{-1}) 3053(m), 3020(m), 2883(m), 1629(vs), 1467(vs), 1423(s), 1406(s), 1371(m), 1321(m), 1245(w), 1184(m), 1119(w), 1095(s), 1027(s), 943(w), 854(m), 825(m), 760(m), 702(s), 629(m). Sodium 4-pyridinemethanethiolate. (0.79 g, 5.37 mmoL, 93% yield) FT-IR (KBr, cm^{-1}) 2948(s), 2912(s), 2841(s), 2771(s), 1632(vs), 1602(vs), 1556(m), 1494(m), 1470(s), 1444(s), 1417(s), 1375(s), 1325(m), 1226(w), 1205(w), 1192(w), 1099(m), 1087(s), 1064(s), 1041(m), 1003(m), 933(w), 921(w), 879(m), 823(m), 748(w), 696(m), 667(w), 599(w), 568(m), 536(w), 480(w).

Phenylmethyl (*p*-cyanobenzyl) Sulfonium Tetrafluoroborate was synthesized according to published method with a modification.[10] Thioanisole (0.62 g, 5 mmoL), α-bromo-*p*-tolunitrile (0.98 g, 5 mmoL), and silver tetrafluoroborate (0.97 g, 5 mmoL) were dissolved CH_2Cl_2 (15 mL). The reaction mixture was stirred at room temperature for 3 days and filtered. Diethyl ether (40 mL) added to the filtrate for crystallization, and the product was obtained as white crystals (1.417 g, 4.33 mmoL, 87% yield). Anal. Calcd for $C_{15}H_{14}BF_4NS$: C, 55.07; H, 4.31; N, 4.28. Found: C, 55.97; H, 4.31; N, 4.20. ^{1}H-NMR (300 MHz, CD_3CN, ppm) 3.19 (s, 1H, $\underline{CH_3}$), 4.81 (d, *J* = 55.7, 12.8 Hz, 2H, S-$\underline{CH_2}$-*p*-C_6H_4CN). FT-IR (KBr, cm^{-1}) 3014(w), 2958(w), 2912(w), 2235(m), 1504(w), 1475(w), 1444(w), 1415(w), 1081(vs), 1070(vs), 1037(vs), 999(w), 973(m), 852(w), 826(w), 785(s), 748(w), 686(m), 555(m), 522(w), 474(w).

(^{n}Bu$_4$N)$_2$[Fe_4S_4(S2-Pic)$_4$] (II). To the solution of (^{n}Bu$_4$N)$_2$[$Fe_4S_4Cl_4$] (**I**, 0.44 g, 0.452 mmoL) in CH_3CN (5 mL), NaS2-Pic (0.26 g, 1.808 mmoL, 4 eq) in CH_3OH was added, and the reaction mixture was stirred for 1 hr. The reaction mixture was filtered to remove insoluble precipitates, and diethyl ether (40 mL) was deposited carefully over the filtrate. After 7 days, black needle-shaped crystals were isolated. (^{n}Bu$_4$N)$_2$[Fe_4S_4(S2-Pic)$_4$]. (0.43 g, 0.32 mmoL, 71% yield). Anal. Calcd for $C_{56}H_{96}Fe_4N_6S_8$: C, 50.45; H, 7.26; N, 6.30. Found: C, 49.80; H, 6.95; N, 6.23. UV-vis (MeCN, nm) λ_{max} (ε) = 398 (12.0 $cm^{-1}mM^{-1}$). FT-IR (KBr, cm^{-1}) 3427(m), 3047(w), 2959(vs), 2935(vs), 2872(vs), 1655(w), 1589(vs), 1564(s), 1479(vs), 1431(vs), 1379(m), 1363(w), 1300(w), 1254(m), 1200(w), 1167(w), 1149(m), 1078(w), 1051(m), 1026(w),

1005(w), 993(w), 885(m), 786(m), 761(s), 711(w), 692(w), 632(w), 582(w), 363(s), 324(s). Cyclic voltammetry (MeCN, vs Ag/AgCl, V) −1.18 (rev).

(^{n}Bu$_4$N)$_2$[Fe$_4$S$_4$(S3-Pic)$_4$] (III). Black plate-shaped crystals. (0.47 g, 0.35 mmoL, 78% yield) Anal. Calcd for $C_{56}H_{96}Fe_4N_6S_8$: C, 50.45; H, 7.26; N, 6.30. Found: C, 49.25; H, 7.25; N, 6.15. UV-vis (MeCN, nm) λ_{max} (ε) = 400 (23.7 $cm^{-1}mM^{-1}$). FT-IR (KBr, cm^{-1}) 3421(w), 3022(w), 2957(vs), 2930(s), 2870(s), 1630(m), 1574(m), 1479(vs), 1420(s), 1379(s), 1232(w), 1213(m), 1190(m), 1149(m), 1099(m), 1026(s), 881(m), 822(m), 804(m), 734(m), 714(s), 694(m), 629(m), 397(w), 382(m), 353(vs). Cyclic voltammetry (MeCN, *vs* Ag/AgCl, V) −1.07 (rev).

(^{n}Bu$_4$N)$_2$[Fe$_4$S$_4$(S4-Pic)$_4$] (IV). Black microcrystalline products. (0.32 g, 0.24 mmoL, 52% yield) Anal. Calcd for $C_{56}H_{96}Fe_4N_6S_8$: C, 50.45; H, 7.26; N, 6.30. Found: C, 49.63; H, 7.05; N, 6.19. UV-Vis (MeCN, nm) λ_{max} (ε) = 395 (22.5 $cm^{-1}mM^{-1}$). FT-IR (KBr, cm^{-1}) 3419(m), 3061(w), 3022(w), 2957(vs), 2932(s), 2870(s), 1597(vs), 1558(w), 1479(vs), 1458(s), 1410(s), 1379(m), 1215(w), 1203(w), 1149(w), 1064(w), 1026(w), 991(m), 879(m), 831(w), 812(w), 736(m), 686(m), 561(m), 478(m), 374(m), 353(vs). Cyclic voltammetry (MeCN, *vs* Ag/AgCl, V) −1.05 (rev).

Reactivity study of complex III. Complex **III** ((^{n}Bu$_4$N)$_2$[Fe$_4$S$_4$(S3-Pic)$_4$], 50 mg, 37.5 μmoL) was dissolved in 2 mL of acetonitrile and (PhMeSCH$_2$-*p*-C$_6$H$_4$CN)(BF$_4$) (12.3 mg, 37.5 μmoL) was added to the solution. The reaction mixture was stirred for 5 min and filtered to remove a black insoluble solid under N_2 at room temperature. The filtrate was dried under vacuum and the residue was isolated by preparative TLC. The isolates were analyzed further by means of ^{1}H NMR and EI-MS spectrometers. EI-MS spectrum of the first product was obtained in MeCN. Molecular ion peak at 124.02 *m/z* confirmed the product as PhSMe. EI-MS$^+$ (MeCN, *m/z*) 124.02 ([C$_6$H$_4$-S-CH$_3$]$^+$), 108.99 ([C$_6$H$_4$-S]$^+$), 78.00 ([C$_6$H$_4$]$^+$). The other product was identified as 3-PicSCH$_2$-*p*-C$_6$H$_4$CN. ^{1}H-NMR (300 MHz, $CDCl_3$, ppm) 3.65 (*s*, 2H, CH_2), 3.71 (*s*, 2H, CH_2), 7.27 (*m*, 1H, Pyr), 7.42 (*m*, 2H, *p*-C$_6$H$_4$CN), 7.64 (*m*, 1H, Pyr), 7.67(*m*, 2H, *p*-C$_6$H$_4$CN), 8.43 (*m*, 2H, Pyr).

X-ray crystallography. Black needle-shaped crystals of the (^{n}Bu$_4$N)$_2$[Fe$_4$S$_4$(S2-Pic)$_4$ (**II**) and black plate-shaped crystals of (^{n}Bu$_4$N)$_2$[Fe$_4$S$_4$(S3-Pic)$_4$ (**III**) were obtained from the slow diffusion of diethyl ether into the MeCN/methanol solutions of each product. All diffraction data were collected at 170(2) K using a Bruker SMART area diffractometer equipped with a monochromator in the Mo Kα (λ = 0.71073 Å) incident beam. The CCD data were integrated and scaled using the Bruker-SAINT software package, and the structures were solved and refined using SHEXTL V5.10.[17] The crystal data and structural parameters are shown in Table 1, and the X-ray crystallographic structures of **II** and **III** are shown in Figures 2 and 3 together with structural information. The structures were solved by direct methods to locate heavy atoms, and the non-hydrogen atoms were located through subsequent difference Fourier syntheses. Structural refinement was carried out by full-matrix least-squares on F^2. Hydrogen atoms were located in the calculated positions. For the structure of **II**, all the non-hydrogen atoms are refined anisotropically, and FLAT command was used for the disordered 2-pyridinemethanthiolate terminal ligands.

Table 1. Crystal data and structure refinements for (^{n}Bu$_4$N)$_2$[Fe$_4$S$_4$(S2-Pic)$_4$] (**II**) and (^{n}Bu$_4$N)$_2$[Fe$_4$S$_4$(S3-Pic)$_4$] (**III**)

	II	**III**
Empirical formula	$C_{56}H_{70}Fe_4N_6S_8$	$C_{56}H_{90}Fe_4N_6S_8$
Formula weight	1307.06	1327.22
Temperature	170(2) K	170(2) K
Wavelength	0.71073 Å	0.71073 Å
Crystal system	Monoclinic	Monoclinic
Space group	*C*2/*c*	*C*2/*c*
Unit cell dimensions	*a* = 24.530(5) Å *b* = 24.636(4) Å *c* = 21.762(4) Å *β* = 103.253(3)°	*a* = 26.0740(18) Å *b* = 23.3195(16) Å *c* = 22.3720(15) Å *β* = 100.467(2)°
Volume	12801(4) Å^3	13376.5(16) Å^3
Z, Calculated density	8, 1.356 Mg/m^3	8, 1.318 Mg/m^3
Absorption coefficient	1.189 mm^{-1}	1.138 mm^{-1}
F(000)	5440	5600
Crystal size	0.35×0.06×0.05 mm	0.20×0.15×0.03 mm
θ range for data collection	1.91 to 26.37°	1.59 to 26.37°
Limiting indices	−30 ≤ h ≤ 27 −30 ≤ k ≤ 27 −26 ≤ l ≤ 27	−32 ≤ h ≤ 18 −29 ≤ k ≤ 29 −24 ≤ l ≤ 27
Reflections collected/ unique	36494/13055	38252/13650
R (int)	0.1220	0.1070
Completeness to theta	26.37°, 99.7%	26.37°, 99.8%
Refinement method	Full-matrix least-squares on F^2	Full-matrix least-squares on F^2
Data / restraints / parameters	13055 / 0 / 630	13650 / 1 / 656
Goodness-of-fit on F^2	0.886	0.784
R indices [I > 2σ(I)]	R1 = 0.0633, wR2 = 0.1544	R1 = 0.0583, wR2 = 0.1406
R indices (all data)	R1 = 0.1333, wR2 = 0.1616	R1 = 0.1380, wR2 = 0.1555
CCDC deposition number	804506	804504

Results and Discussion

Synthesis.

(^{n}Bu$_4$N)$_2$[Fe$_4$S$_4$(SR)$_4$] (R = 2-Pic (II), 3-Pic (III), and 4-Pic (IV)) Clusters. Syntheses of complexes **II**, **III**, and **IV** were achieved by thermodynamics-driven ligand substitution reaction of complex **I** by using the corresponding sodium salts of pyridinemethanthiol. Sodium pyridinemethanethiolate in MeOH was added dropwise to the MeCN solution of **I**. From the reaction mixture, the insoluble byproducts including NaCl were removed by filtration. Ligand substitution is the other synthetic method for the synthesis of new M/Fe/S

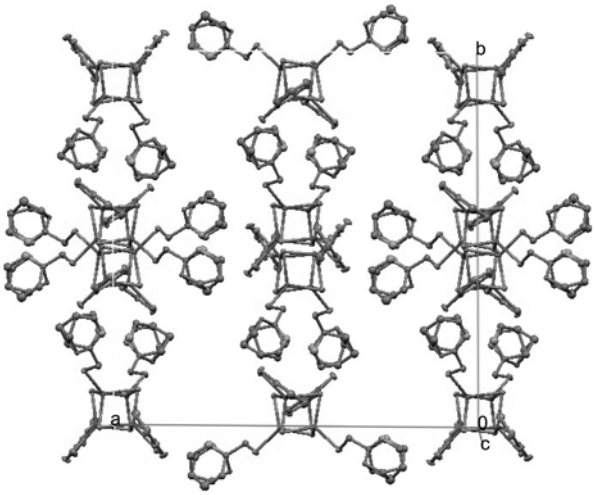

Figure 1. Packing plot of (^{n}Bu$_4$N)$_2$[Fe$_4$S$_4$(S2-Pic)$_4$] (**II**), rendered by Mercury 2.4 software, shows [Fe$_4$S$_4$(S2-Pic)$_4$]$^{2-}$ core. Counter cations and hydrogen atoms were omitted for clarity.

clusters. For examples, introduction of the phosphine and CO ligands often resulted in the new clusters because these ligands prefer lower oxidation state of the cluster and lead to the incomplete terminal ligand substitution or cluster core rearrangement.[18] However, ligand substitutions from chloride to thiolate are known to have no such effect.[19] Crystallization of the products was performed by layering diethyl ether over the reaction filtrate. After a few days, black crystalline products of complexes **II**, **III**, and **IV** were obtained and which were used for the characterizations and X-ray crystallography.

Structural Description. The structure of (^{n}Bu$_4$N)$_2$[Fe$_4$S$_4$(S2-Pic)$_4$] (**II**) was characterized in monoclinic *C*2/*c* space group with *Z* = 8 at 170(2) K, and the unit cell contains two independent molecules of complex **II** (Figure 1). A distinct difference between two molecules is the position of 2-pyridinethiolate terminal ligands, and of which pyridyl groups are found to be axial (Figure 2(a)) and equatorial when we compare relative position of both pyridyl groups with the Fe$_4$S$_4$ core (Figure 2(b)). Formation of two different structures of complex **II** in the unit cell appears to be due to the bidentate-mode coordination by two 2-pyridinemethanethiolates and the flexibility of the pyridyl group. Torsional angle of S2-Fe2-S4-C7 in Figure 2(a) and that of S6-Fe4-S8-C19-C20 in Figure 2(b) are 84.35° and 40.76°, respectively. This is a rare example that shows conformational changes of the cluster ligands in the solid state structure, even though it may partly be due to the crystal packing effect.

Two different conformations of complex **II** seem to influence the [Fe$_4$S$_4$]$^{2+}$ core structure too. Two Fe-Fe distances of Fe1-Fe1# (3.076(2) Å) and Fe2-Fe2# (2.716(2) Å) in **IIA** are significantly shorter than those of Fe3-Fe3# (3.104(2) Å) and Fe4-Fe4# (2.7273(19) Å) in **IIB**. On the contrary, the other Fe-Fe distances between pentacoordinated and hexacoordinated Fe atoms show the opposite tendency. The distances of Fe1-Fe2 (2.8940(14) Å) and Fe1-Fe2# (2.8024(15) Å) are significantly longer than the corresponding Fe3-Fe4 (2.8758(14) Å) and Fe3-Fe4# (2.7856(15) Å). The average Fe-Fe distance of complex **II** is 2.862 Å, and that is much longer than the other [Fe$_4$S$_4$(SR)$_4$]$^{2-}$ clusters. The average Fe-Fe distances of the (Et$_4$N)$_2$[Fe$_4$S$_4$(SCH$_2$Ph)$_4$] and the (Et$_4$N)$_2$[Fe$_4$S$_4$(SPh)$_4$] clusters are 2.747 Å[20] and 2.736 Å,[21] respectively. The average distance of Fe-μ_3-S of complex **II** is 2.322 Å, and which is also significantly longer than that of the (Et$_4$N)$_2$[Fe$_4$S$_4$(SCH$_2$Ph)$_4$] and the (Et$_4$N)$_2$[Fe$_4$S$_4$(SPh)$_4$] (both 2.286 Å). Therefore, extra coordination at the Fe centers of complex **II** has weakened the Fe-Fe interactions in the Fe$_4$S$_4$ core and eventually increased the core size.

The (^{n}Bu$_4$N)$_2$[Fe$_4$S$_4$(S3-Pic)$_4$] (**III**) complex was also crystallized in the monoclinic *C*2/*c* space group with *Z* = 8 and the structure is shown at Figure 3. The average Fe-Fe distance of complex **III** is 2.731 Å and which is shorter by 0.131 Å than that of complex **II**. Compared to the (Et$_4$N)$_2$[Fe$_4$S$_4$(SCH$_2$Ph)$_4$] cluster, the Fe-Fe distance is still 0.016 Å

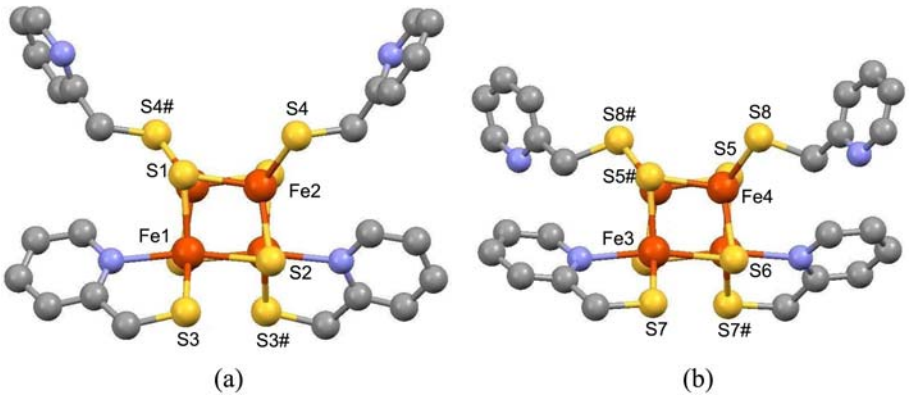

Figure 2. Two independent crystallographic structures of (^{n}Bu$_4$N)$_2$[Fe$_4$S$_4$(S2-Pic)$_4$] (**II**); counter cations and hydrogen atoms were omitted for clarity. Structure A: Fe(1)-Fe(1)#; 3.076(2) Å, Fe(1)-Fe(2); 2.8940(14) Å, Fe(1)-Fe(2)#; 2.8024(15) Å, Fe(2)-Fe(1)#; 2.8024(15) Å, Fe(2)-Fe(2)#; 2.716(2) Å, Fe(1)-S(1); 2.320(2) Å, Fe(1)-S(2); 2.446(2) Å, Fe(1)-S(2)#; 2.310(2) Å, Fe(2)-S(1); 2.313(2) Å, Fe(2)-S(1)#; 2.301(2) Å, Fe(2)-S(2); 2.245(2) Å, Fe(1)#-S(2); 2.310(2) Å, Fe(1)-S(3); 2.328(2) Å, Fe(1)-N(1); 2.287(6) Å, Fe(2)-S(4); 2.300(2) Å. Structure B: Fe(3)-Fe(3)#; 3.104(2) Å, Fe(3)-Fe(4); 2.8758(14) Å, Fe(3)-Fe(4)#; 2.7856(15) Å, Fe(4)-Fe(3)#; 2.7856(15) Å, Fe(4)-Fe(4)#; 2.7273(19) Å, Fe(3)-S(5)#; 2.304(2) Å, Fe(3)-S(6); 2.4513(19) Å, Fe(3)-S(6)#; 2.319(2) Å, Fe(4)-S(5); 2.321(2) Å, Fe(4)-S(5)#; 2.301(2) Å, Fe(4)-S(6); 2.228(2) Å, Fe(3)#-S(6); 2.319(2) Å, Fe(3)-S(7); 2.325(2) Å, Fe(3)-N(3); 2.311(6) Å, Fe(4)-S(8); 2.304(2) Å.

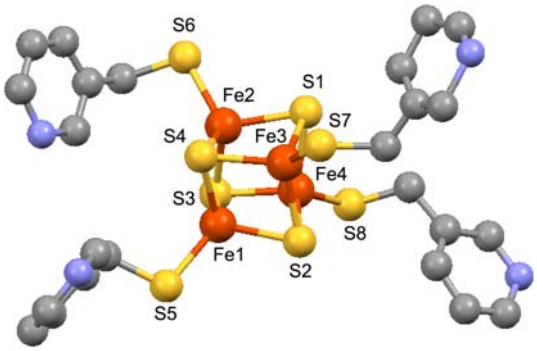

Figure 3. Crystallographic structure of (^{n}Bu$_4$N)$_2$[Fe$_4$S$_4$(S3-Pic)$_4$] (**III**); counter cations and hydrogen atoms were omitted for clarity. Fe(1)-Fe(2); 2.7592(10) Å, Fe(1)-Fe(3); 2.7004(10) Å, Fe(1)-Fe(4); 2.7256(10) Å, Fe(2)-Fe(3); 2.7181(10) Å, Fe(2)-Fe(4); 2.7033(13) Å, Fe(3)-Fe(4); 2.7813(11) Å, Fe(1)-S(2); 2.2518(16) Å, Fe(1)-S(3); 2.2942(13) Å, Fe(1)-S(4); 2.2916(16) Å, Fe(2)-S(1); 2.2486(17) Å, Fe(2)-S(3); 2.3011(17) Å, Fe(2)-S(4); 2.2878(14) Å, Fe(3)-S(1); 2.2875(14) Å, Fe(3)-S(2); 2.2986(17) Å, Fe(3)-S(4); 2.2433(16) Å, Fe(4)-S(1); 2.3160(17) Å Fe(4)-S(2); 2.2812(13) Å Fe(4)-S(3); 2.2509(16) Å, Fe(1)-S(5); 2.2492(13) Å, Fe(2)-S(6); 2.2492(18) Å Fe(3)-S(7); 2.2431(16) Å Fe(4)-S(8); 2.2545(18) Å.

shorter. The average Fe-μ_3-S distance of complex **III** is 2.279 Å and also slightly shorter than that of the (Et$_4$N)$_2$[Fe$_4$S$_4$(SCH$_2$Ph)$_4$] and the (Et$_4$N)$_2$[Fe$_4$S$_4$(SPh)$_4$] complexes. The comparison between complex **III** and the (Et$_4$N)$_2$[Fe$_4$S$_4$(SCH$_2$Ph)$_4$] cluster showed the effects on the structural changes resulted from the pyridyl group substitution of phenyl group. Overall, the core size was reduced as reflected from the Fe-Fe and Fe-μ_3-S bond distances changes. It is well established that LUMO of the [Fe$_4$S$_4$]$^{2+}$ core is the molecular bonding orbital, and it was confirmed that the reduction of [Fe$_4$S$_4$]$^{2+}$ clusters reduced core size by extending metal-metal interactions.[22] Hence, the pyridyl group of complex **III** seems to donate more electron density to the [Fe$_4$S$_4$]$^{2+}$ core.

Because of the small crystal size, X-ray structure of complex **IV** could not be obtained. When Cu Kα X-ray beam (1.54187 Å) equipped diffractometer was used for the black plate-shaped crystals of (^{n}Bu$_4$N)$_2$[Fe$_4$S$_4$(S4-Pic)$_4$ (**IV**), low resolution structure was obtained. Even though the quality of X-ray structure was not publishable, preliminary structure of **IV** showed similar core structure and ligand coordination to the refined structure of complex **III** (Table 1S, Figure 1S).

Physical Properties. Fe/S clusters have distinct UV-vis absorptions depending on the core structure and redox states, and they often are used for the characterization of biological Fe/S clusters.[23] The UV-vis spectrum of the [Fe$_4$S$_4$Cl$_4$]$^{2-}$ (**I**) cluster in MeCN found two λ_{max} at 504 nm (ε = 1.55 cm^{-1} mM^{-1}) and 692 nm (ε = 1.26 cm^{-1}mM^{-1}), which was similar to the reported absorptions attributed to the Cl $\rightarrow$ core charge-transfer excitations.[15,24] UV-vis spectral change upon ligand substitution is shown at Figure 4, and the new absorption at 400 nm (ε = 23.7 cm^{-1}mM^{-1}) was observed with complex **III** in MeCN. Due to the ligand substitution from chloride to thiolate, blue shift of the S $\rightarrow$ core charge-transfer transition band took place. Complex **IV** showed

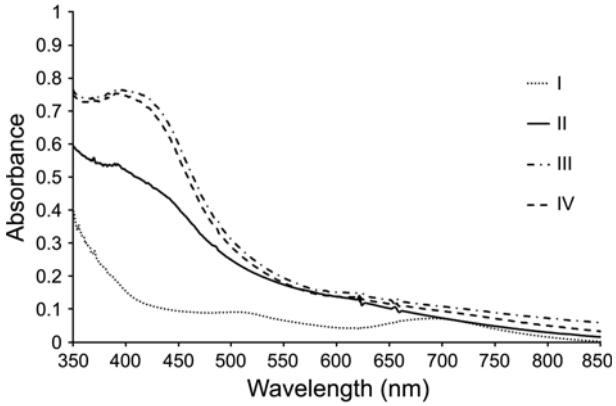

Figure 4. UV-vis spectra of complex **I**, **II**, **III**, and **IV** in MeCN.

similar electronic absorption to complex **III** with λ_{max} at 395 nm (ε = 22.5 cm^{-1} mM^{-1}). The similar phenomena are observed in the other similar clusters, [Fe$_4$S$_4$(SCH$_2$Ph)$_4$]$^{2-}$, and [Fe$_4$S$_4$(SPh)$_4$]$^{2-}$, of which λ_{max} were reported at 420 nm (ε = 18.5 cm^{-1}mM^{-1} in DMF) and 457 nm (ε = 17.7 cm^{-1}mM^{-1} in DMF), respectively.[25] However, the 2:2 site-differentiated cluster **II** showed λ_{max} at 398 nm with much lower intensity (ε = 12.0 cm^{-1}mM^{-1}). It seems the extra coordination ligands reduce the intensity of ligand to [Fe$_4$S$_4$]$^{2+}$ core charge-transfer electronic absorption.

Because the ligand-substituted complexes **II**, **III**, and **IV** have pyridine ring, the new ν(C$_{sp^2}$-H) peaks and the strong ν(C=N) absorptions, missing from the starting (Et$_4$N)$_2$[Fe$_4$S$_4$Cl$_4$] (**I**) complex, were observed from infrared spectra at the region of 3020-3060 cm^{-1} and at 1558-1655 cm^{-1}, respectively (Figure 2S). Characteristic IR peaks of the common ^{n}Bu$_4$N$^+$ cation in the complexes are found at 2957, 2930, 2870 and 1479-600 cm^{-1}. Significant structural changes in the [Fe$_4$S$_4$]$^{2+}$ core of complex **II** was detected by far-range infrared spectroscopy (Figure 3S). Strong absorptions observed at 353 cm^{-1} for complexes **I**, **III**, and **IV** are corresponding to the Fe-μ_3-S stretching transitions.[26,27] The same infrared transition for the [Fe$_4$S$_4$(SCH$_2$Ph)$_4$]$^{2-}$ cluster was reported to be found at 359 cm^{-1} at 77 K.[28] However, in the case of complex **II**, the corresponding peak was observed at 363 cm^{-1} and 324 cm^{-1} due to the two different Fe coordination geometries.

Reduction potential changes by ligand substitution have been studied by cyclic voltammetry. The complex **I** in

Table 2. Redox potentials of the [Fe$_4$S$_4$]$^{2+}$ clusters. The potential reported *vs.* Ag/AgCl as a reference electrode

Compounds	$E_{1/2}$ (V)
(Et$_4$N)$_2$[Fe$_4$S$_4$(SCH$_2$Ph)$_4$]	−1.15 (rev)[a]
(Et$_4$N)$_2$[Fe$_4$S$_4$(SPh)$_4$]	−0.94 (rev)[a]
(^{n}Bu$_4$N)$_2$[Fe$_4$S$_4$Cl$_4$] (**I**)	−0.74 (rev)
(^{n}Bu$_4$N)$_2$[Fe$_4$S$_4$(S2-Pic)$_4$] (**II**)	−1.18 (rev)
(^{n}Bu$_4$N)$_2$[Fe$_4$S$_4$(S3-Pic)$_4$] (**III**)	−1.07 (rev)
(^{n}Bu$_4$N)$_2$[Fe$_4$S$_4$(S4-Pic)$_4$] (**IV**)	−1.05 (rev)

[a]corrected values *vs.* Ag/AgCl.

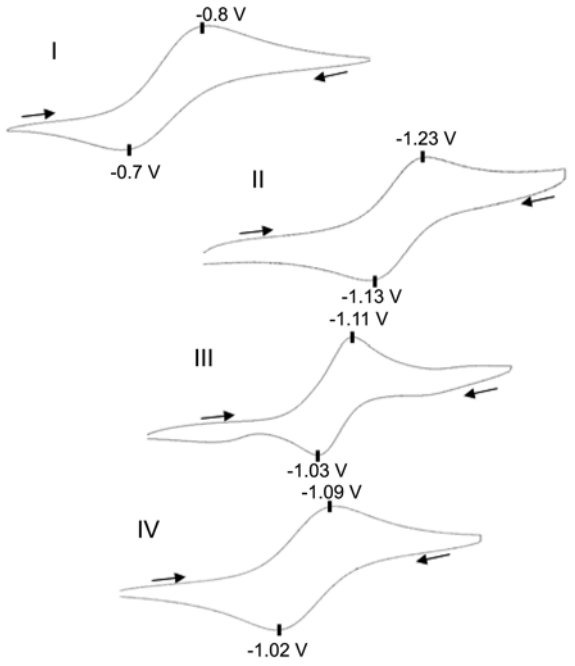

Figure 5. Cyclic voltammograms of (^{n}Bu$_4$N)$_2$[Fe$_4$S$_4$Cl$_4$] (**I**), [(^{n}Bu$_4$N)$_2$[Fe$_4$S$_4$(S2-Pic)$_4$] (**II**), (^{n}Bu$_4$N)$_2$[Fe$_4$S$_4$(S3-Pic)$_4$] (**III**) and (^{n}Bu$_4$N)$_2$[Fe$_4$S$_4$(S4-Pic)$_4$] (**IV**) at a scan rate of 100 mV/s. Supporting electrolyte: 0.1 M ^{n}Bu$_4$NPF$_6$.

MeCN showed reversible redox reaction and a half-wave potential, corresponding to the $[Fe_4S_4]^{2+}/[Fe_4S_4]^{+}$ couple was found at −0.74 V (*vs*. Ag/AgCl) (Table 2, Figure 5). When the chloride ligand was substituted by pyridinethiolate ligands, the reduction waves of complexes **II**, **III**, and **IV**, corresponding to the $[Fe_4S_4]^{2+}/[Fe_4S_4]^{+}$ couple, were found at much lower values. Benzylthiolate and phenylthiolate substitutions of complex **I** shifted the potential by −0.41 V and −0.20 V, respectively (Table 2). Qualitatively, the thiolate ligands, including alkylthiolate, seem to donate more electron density to the $[Fe_4S_4]^{2+}$ core than chloride does, and that makes reduction of the $[Fe_4S_4]^{2+}$ cluster more difficult.[29] As shown at Table 2, the reduction potentials of the pyridinethiolate complexes were all reversible, and the half-wave potential shift to negative direction in the order of complex **IV**, **III**, and **II**. Compared with $[Fe_4S_4(SCH_2Ph)_4]^{2-}$, the $[Fe_4S_4]^{2+}/[Fe_4S_4]^{+}$ redox couple of complexes **III** and **IV** showed positive shift by 80 mV and 100 mV, respectively. The redox potential changes can also be explained by structural difference.[22] Because the $[Fe_4S_4]^{2+}$ core of complex **III** showed significantly short Fe-Fe and Fe-μ_3-S distances compared to that of the $[Fe_4S_4(SCH_2Ph)_4]^{2-}$ complex, the complex **III** poises the structure that similar to the reduced cluster. Structure similar to the reduction product makes easier reduction of the cluster, and higher reduction potential is observed. Same rationale can be used for the explanation of lower reduction potential of complex **II**. Because the $[Fe_4S_4]^{2+}$ core of complex **II** is much larger than that of the $[Fe_4S_4(SCH_2Ph)_4]^{2-}$ complex due to the bidentate ligation of S2-Pic, the complex **II** needs to experience larger structural changes which requires high energy.

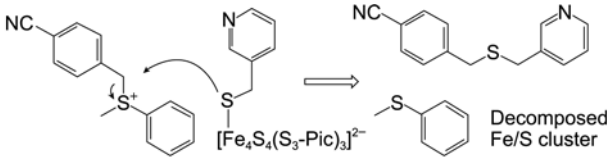

Figure 6. Proposed reaction pathway for the sulphonium cleavage by complex **III**.

Therefore, the pyridyl substitutions of phenyl group of the $[Fe_4S_4(SCH_2Ph)_4]^{2-}$ complex donate more electron density to the core and reduce the $[Fe_4S_4]^{2+}$ core size, and that results in the positive shift of reduction potentials. When the coordination number of the $[Fe_4S_4]^{2+}$ core increases as shown in **II**, the Fe-Fe and Fe-μ_3-S distances increase and the reduction potential shift to the negative direction.

Reactivity of Fe/S Cluster in the Sulfonium Cleavage. Because the Fe/S cluster in the radical SAM enzymes is known to generate the radical species from biological sulphonium, SAM.[8] The reaction between complex **III** and $[PhMeSCH_2$-*p*-$C_6H_4CN]^{+}$ sulfonium was investigated. The reaction mixture was added with diethyl ether to precipitate Fe/S cluster, and the organic products in solution was checked by silica gel TLC. Two major products were isolated by preparative TLC, and identified by EI-MS and ^{1}H NMR. One of products was thioanisole, confirmed by TLC (Figure 4S) and EI-MS (Figure 5S). 3-PicSCH_2-*p*-C_6H_4CN was identified as the other product by ^{1}H-NMR. The peaks for pyridine ring of 3-pyridinethiolate were observed at 7.27 ppm, 7.64 ppm, and 8.43 ppm and two sets of *p*-C_6H_4CN protons at 7.42 ppm and 7.67 ppm. No compound may be formed by the radical reaction was detected.

The $[Fe_4S_4(S3\text{-}Pic)_4]^{2-}$ complex (**III**) was able to cleavage the $[PhMeSCH_2$-*p*-$C_6H_4CN]^{+}$ sulphonium, and PhSMe and 3-PicSCH_2-*p*-C_6H_4CN were identified as products. The reaction can be explained as an electrophilic type cleavage of the sulphonium by pyridinethiolate without any redox reaction (Figure 6).[30] Radical SAM enzymes containing the $[Fe_4S_4]^{2+}$ cluster are known to generate 5'-deoxyadenosyl radical through the cleavage of sulphonium SAM after reduction to the $[Fe_4S_4]^{+}$ cluster.[31] Because the reduction potential of complex **III** is too low, radical generation by the complex **III** does not appear feasible.

Acknowledgments. This research was supported by Basic Science Research Program through the National Research Foundation of Korea (NRF) funded by the Ministry of Education, Science and Technology (2010-0020984). The authors thank to Prof. Youngmee Kim at Ewha Womans University in Korea and Jeff W. Kampf at University of Michigan for the X-ray crystallographic data collections.

Appendix A. Supplementary Data. Crystallographic table and structure of **IV**, FT-IR spectra of the complexes, and characterization of sulphonium cleavage reaction products are included. CCDC 804506 and 804504 contain the supplementary crystallographic data for the complex **II** and

III. These data can be obtained free of charge *via* http://www. ccdc.cam.ac.uk/conts/retrieving.html, or from the Cambridge Crystallographic Data Centre, 12 Union Road, Cambridge CB2 1EZ, UK; fax: (+44) 1223-336-033; or e-mail: deposit @ccdc.cam.ac.uk. Supplementary data associated with this article can be found, in the online version, at doi: http://dx.doi.org/10.5012/bkcs.2012.33.1.48.

References

1. Kim, M.; Han, J. *Polyhedron* **2007**, *26*, 2949.
2. Lee, S. C.; Holm, R. H. *Chem. Rev.* **2004**, *104*, 1135.
3. Han, J.; Beck, K.; Ockwig, N.; Coucouvanis, D. *J. Am. Chem. Soc*. **1999**, *121*, 10448.
4. Zhou, J.; Holm, R. H. *J. Am. Chem. Soc*. **1995**, *117*, 11353.
5. Barton, B. E.; Whaley, C. M.; Rauchfuss, T. B.; Gray, D. L. *J. Am. Chem. Soc.* **2009**, *131*, 6942.
6. Lee, C. M.; Chen, C. H.; Liao, F. X.; Hu, C. H.; Lee, G. H. *J. Am. Chem. Soc*. **2010**, *132*, 9256.
7. Gräwert, T.; Rohdich, F.; Span, I.; Bacher, A.; Eisenreich, W.; Eppinger, J.; Groll, M. *Angew. Chem*. **2009**, *48*, 5756.
8. Frey, P. A.; Hegeman, A. D.; Ruzicka, F. J. *Crit. Rev. Biochem. Mol. Biol*. **2008**, *43*, 63.
9. Schnell, R.; Sandalova, T.; Hellman, U.; Lindqvist, Y.; Schneider, G. *J. Biol. Chem*. **2005**, *280*, 27319.
10. Saeva, F. D.; Morgan, B. P. *J. Am. Chem. Soc*. **1984**, *106*, 4121.
11. Shin, B. K.; Kim, M.; Han, J. *Polyhedron*. **2010**, *29*, 2560.
12. Kim, M.; Chi, Y. S.; Han, J. *Bull. Korean Chem. Soc*. **2010**, *31*, 23.
13. Shin, B. K.; Kim, Y.; Kim, M.; Han, J. *Polyhedron*. **2007**, *26*, 4557.
14. Kim, M.; Kim, Y. U.; Han, J. *Polyhedron*. **2007**, *26*, 4003.
15. Wong, G. B.; Bobrik, M. A.; Holm, R. H. *Inorg. Chem*. **1978**, *17*, 578.
16. Remuzon, P.; Bouzard, D.; Cesare, P. D.; Essiz, M.; Jacquet, J. P.; Nicolau, A. *Tetrahedron*. **1995**, *51*, 9657.
17. Sheldrick, G. M. *Acta Crystallogr. A*. **2008**, *64*, 112.
18. Han, J.; Coucouvanis, D. *Inorg. Chem*. **2002**, *41*, 2738.
19. Johnson, R. W.; Holm, R. H. *J. Am. Chem. Soc*. **1978**, *100*, 5338.
20. Averill, B. A.; Herskovitz, T.; Holm, R. H. *J. Am. Chem. Soc*. **1973**, *95*, 3523.
21. Bobrik, M. A.; Hodgson, K. O.; Holm, R. H. *Inorg. Chem*. **1977**, *16*, 1851.
22. Dey, A.; Jenney, F. E., Jr.; Adams, M. W. W.; Babini, E.; Takahashi, Y.; Fukuyama, K.; Hodgson, K. O.; Hedman, B.; Solomon, E. I. *Science* **2007**, *318*, 1464.
23. Frankel, R. B.; Herskovitz, T.; Averill, B. A.; Holm, R. H.; Krusic, P. J.; Phillips, W. D. *Biochem. Biophys. Res. Comm*. **1974**, *58*, 974.
24. Kanatzidis, M. G.; Hagen, W. R. Dunham, W. R.; Lester, R. K.; Coucouvanis, D. *J. Am. Chem. Soc.* **1985**, *107*, 953.
25. DePamphilis, B. V.; Averill, B. A.; Herskovitz, T.; Que, L., Jr.; Holm, R. H. *J. Am. Chem. Soc*. **1974**, *96*, 4159.
26. Kern, A.; Näther, C.; Tuczek, F. *Inorg. Chem*. **2004**, *43*, 5020.
27. Xiao, Y.; Koutmos, M.; Case, D. A.; Coucouvanis, D.; Wang, H.; Cramer, S. P. *Dalton Trans.* **2006**, 2192.
28. Czernuszewicz, R. S.; Macor, K. A.; Johnson, M. K.; Gewirth, A.; Spiro, T. G. *J. Am. Chem. Soc*. **1987**, *109*, 7178.
29. Cambray, J.; Lane, R. W.; Wedd, A. G.; Johnson, R. W.; Holm, R. H. *Inorg. Chem*. **1977**, *16*, 2565.
30. Daley, C. J. A.; Holm, R. H. *Inorg. Chem*. **2001**, *40*, 2785.
31. Walsby, C. J.; Ortillo, D.; Yang, J.; Nnyepi, M. R.; Broderick, W. E.; Hoffman, B. M.; Broderick, J. B. *Inorg. Chem*. **2005**, *44*, 727.